ERCB/AGS Open File Report 2013-01

LiDAR-Based Landslide Classification and Inventory, Peace River, Alberta (NTS 84C)

Energy Resources Conservation Board

Alberta Geological Survey

ERCB/AGS Open File Report 2013-01

LiDAR-Based Landslide Classification and Inventory, Peace River, Alberta (NTS 84C)

A.J. Morgan, D. Chao, and C.R. Froese

Energy Resources Conservation Board
Alberta Geological Survey

February 2013

ISBN 978-1-4601-0091-2

Morgan, A.J., Chao, D. and Froese, C.R. (2013): LiDAR-based landslide classification and inventory, Peace River, Alberta (NTS 84C); Energy Resources Conservation Board, ERCB/AGS Open File Report 2013-01, 22 pp.

Published February 2013 by:
Energy Resources Conservation Board
Alberta Geological Survey
4th Floor, Twin Atria Building
4999 – 98th Avenue
Edmonton, AB T6B 2X3
Canada

Tel: 780.422.1927
Fax: 780.422.1918
E-mail: AGS-Info@ercb.ca
Website: www.ags.gov.ab.ca

Contents

Tables

Figures

Acknowledgements

This work was funded by the Alberta Geological Survey Landslide Inventory Project and by contributions from the Town of Peace River, Alberta Transportation, ATCO Pipelines, ATCO Electric, and Canadian National Railway company. M. Jaboyedoff, T. Shipman, and T. Lemay critically read this paper, and the authors wish to thank them for their comments and suggestions.

Abstract

This open file report discusses the method used to define discrete landslide boundaries within a 100 km^2 study area centred at the Town of Peace River, and also introduces preliminary work investigating the relationship between surface roughness derived from bare-earth light detection and ranging (LiDAR) and landslide activity. Field-based mapping and remote sensing data sources such as LiDAR and airphoto imagery provide a means with which to classify each landslide based on its characteristics, using the nomenclature suggested by Cruden and Varnes (1996). Statistical methods based on the geographic information system (GIS) are applied to a LiDAR digital elevation model (DEM) to produce derivative maps depicting the distribution of slope angle, surface roughness, and slope convexity of each landslide surface. The spatial information provided by these derivative maps is applied in an attempt to understand the relative level of landslide activity in the absence of displacement data. This report details the preliminary work using GIS-based spatial analysis techniques and can be considered the initial steps for an ongoing study in which these methods are being refined and improved. The ultimate goal is to apply a robust spatial analysis technique to other river valley systems where instability is known to occur.

1 Introduction

The Alberta Geological Survey (AGS), with the support of various stakeholders, has initiated a multidisciplinary geohazard study of the Town of Peace River, Alberta, to develop a better understanding of the types and extent of landsliding within the Peace River valley. Interpretation of the geological setting for landslides in the study area produced an updated geological model of the Cretaceous bedrock and Paleogene and Quaternary sediments that are found in the subsurface at the Town of Peace River (Morgan et al., 2012).

Continuing with the Peace River project research, this report discusses the methods used to describe the large-scale landsliding across the project site. To achieve this, landslides are assigned boundaries based on morphology and classified using the nomenclature outlined by Cruden and Varnes (1996). Statistical techniques based on the geographic information system (GIS) are implemented to supplement the morphological classification and refine it where appropriate. Spatial analysis methods are used in an attempt to learn about relative levels of landslide activity within the study area in the absence of measured displacement data and to assess the GIS-based technique for similar applications at other sites.

Only large, deep-seated landslides are considered in this report. A number of smaller slides, seated in colluvium along the river valley slopes, also affect the infrastructure at localized areas at the Town of Peace River, but were not evaluated as part of this work.

2 Geological Setting of Study Area

The Town of Peace River is in northwestern Alberta within NTS area 84C (Figure 1) and lies within the Peace River Lowlands physiographic zone (Pettapiece, 1986). The study area involves a 100 km^2 area approximately centred on the townsite (shown as 'LiDAR Area' in Figure 1). Surface morphology in the area is the result of Paleogene fluvial erosion and sediment deposition, subsequent sediment deposition by the Late Wisconsinan Laurentide Ice Sheet, and Holocene fluvial erosion. The Peace River valley is the dominant geomorphic feature of the region, which evolved as the Peace River incised the Quaternary sediments through Paleogene deposits and into the Cretaceous bedrock. Two other river systems drain into the Peace River: the Heart River, which is located within the study area, and the Smoky River, located just south of the study area (Figure 1).

Bedrock units relevant to landsliding at the townsite consist of the Peace River Formation sandstones, which are overlain by Shaftesbury Formation marine shale and the sandstone of the Dunvegan Formation. The current-day Peace River generally follows a wider and broader preglacial valley that eroded through the Dunvegan Formation into the Shaftesbury Formation, and in some areas through the Shaftesbury shale into the Paddy and Cadotte members of the Peace River sandstones below. This preglacial valley is infilled with a sequence of up to 200 m of sediment, including gravels, sands, silts, clays, and glacial till. Figure 2 shows a synthesized cross-section A–A′ through the study area and is depicted in plan in Figure 1.

Morphological study coupled with detailed corehole logs through these valley infill sediments indicate that many of the large-scale landslides have failure surfaces seated within a deposit of glaciolacustrine clay, which was deposited prior to, and subsequently overridden by, the Laurentide Ice Sheet. Further details of the stratigraphy as it relates to landsliding is presented in Section 3.2.1. A detailed description of the geology at the Town of Peace River is provided in Morgan et al. (2009), which details the results of an AGS drill program. In addition, readers can reference Morgan et al. (2012), which discusses the geological setting for landsliding at the Town of Peace River and includes a more detailed discussion of the data sources for the synthesized cross-section (Figure 2) as well as a detailed stratigraphic chart of the sediments that infill the preglacial river valley and overlie the bedrock formations.

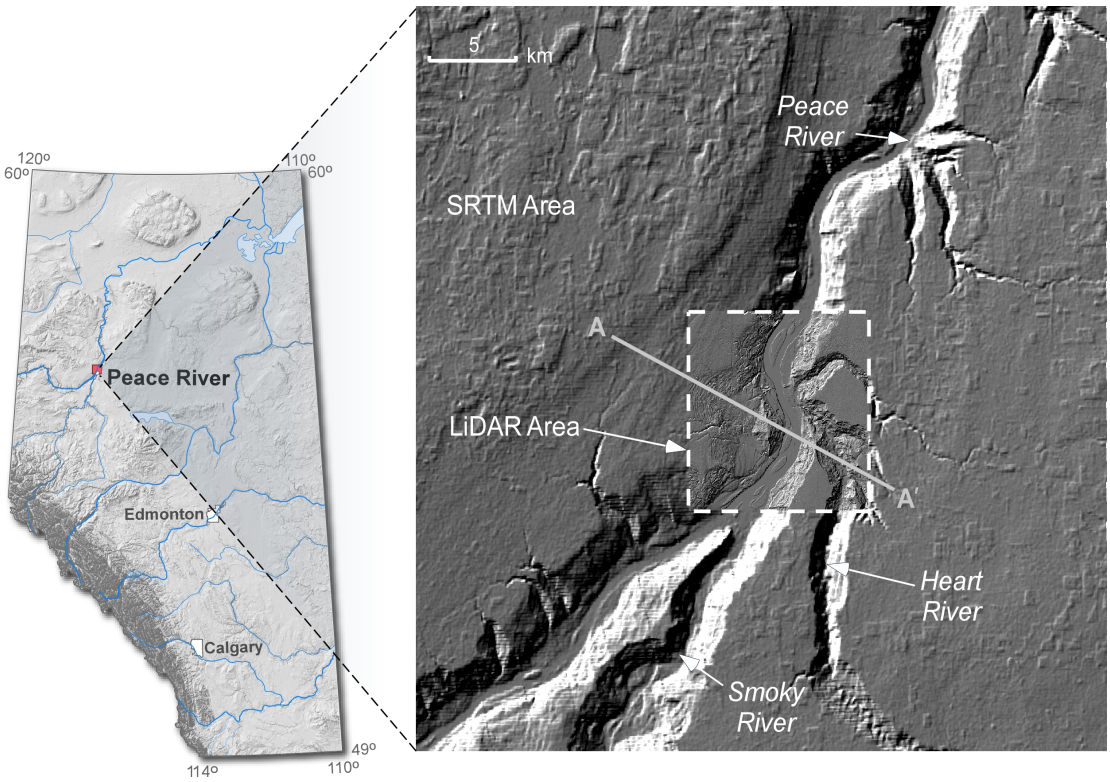

Figure 1. Shaded light detection and ranging (LiDAR) digital elevation model (DEM) of the landslide inventory study area (dashed line) and surrounding Shuttle Radar Topography Mission (SRTM) DEM, west-central Alberta. UTM boundaries of the LiDAR area are 476028E (left), 486198E (right), 6236843N (top), and 6226338N (bottom), Zone 11, NAD83. The shaded images were created using a sun inclination of 40° and an azimuth of 315°. Line A–A' refers to the cross-section depicted in Figure 2. (Figure modified from Morgan et al., 2012)

3 Methodology

3.1 Landslide Selection

Light detection and ranging (LiDAR) data was collected using an Optech 3100 LiDAR system with a pulse rate of 70 kHZ, a scan frequency of 33 Hz, a scan angle of ±25 degrees, and a point spacing of 0.75 m. The LiDAR data was purchased pre-processed and a bare-earth derivative with a 1 m horizontal resolution free of vegetation and man-made structures was used as the DEM for landslide study purposes. Detailed morphological analysis of this DEM was utilized to visually select boundaries for landslides that occur on the river valley slopes throughout the 100 km^2 study area.

A number of shaded-relief images highlighting different aspects of the slide masses were created from the LiDAR DEM in ArcGIS. Images were generated with sun azimuths ranging from 0 to 360 degrees using 45 degree increments (i.e. 0°, 45°, 90°, etc.) and a sun inclination of 45 degrees. The resulting series of shaded-relief images allowed the morphology of the river valley slopes to be examined at a very fine resolution. These shaded-relief images were also visualized in three dimensions in ArcScene using a vertical exaggeration of 3:1. The next step was to develop boundaries for each landslide using expert judgement based on an idealized landslide morphology taken from Cruden and Varnes (1996).

Field reconnaissance carried out over two summers at the site assisted the creation of landslide boundaries, or polygons in ArcGIS. Fieldwork was primarily focused on understanding the stratigraphy at the project site, especially as it relates to landsliding. In addition, general observations of landslide geometry and activity were made, especially where recent movement was obvious.

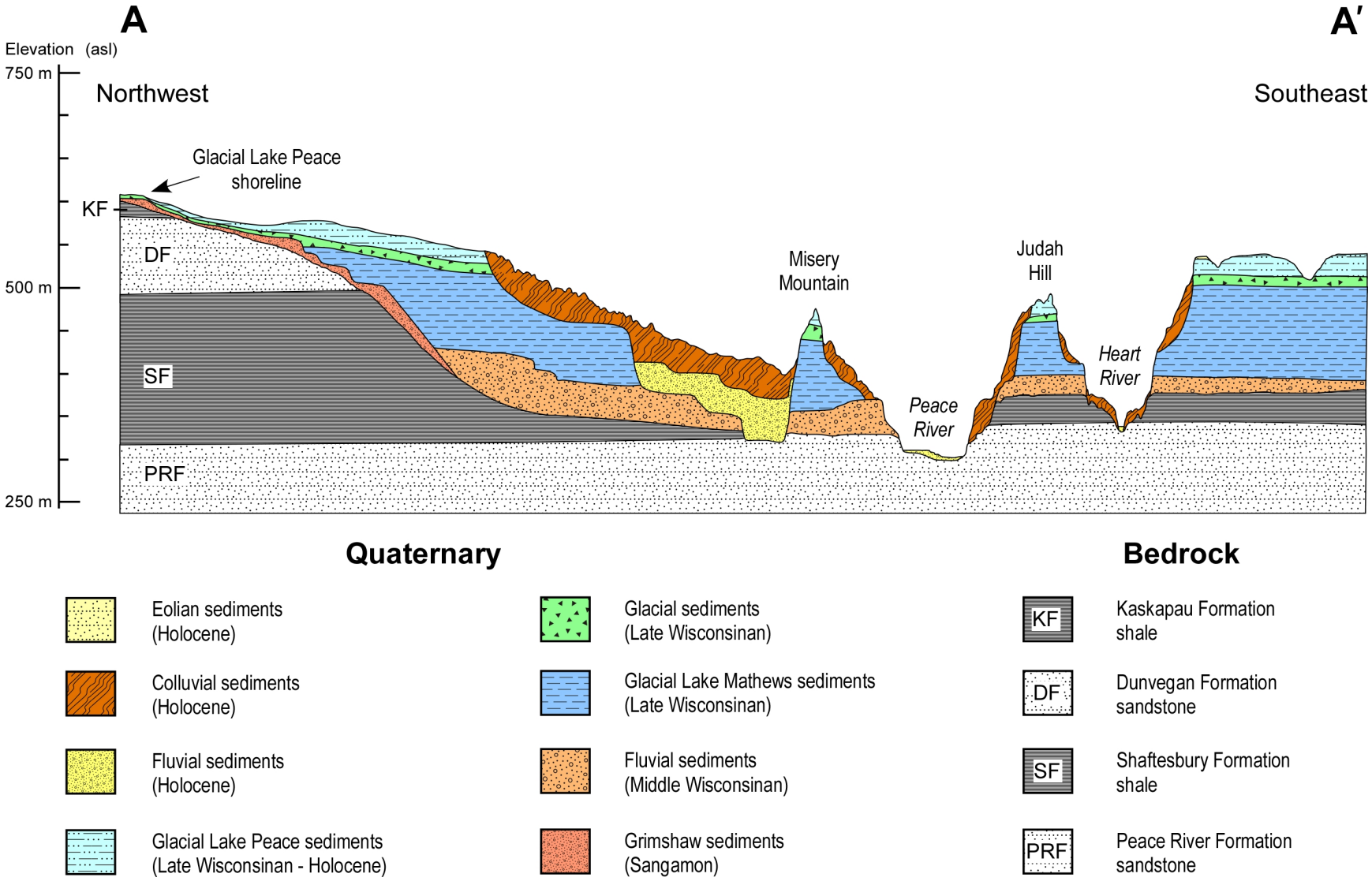

Figure 2. Vertical cross-section through the study area showing bedrock surface and overlying sediments infilling the preglacial valley, west-central Alberta. The location of the cross-section line is shown in Figure 1 (Figure taken from Morgan et al., 2012).

Colour satellite imagery, as well as orthorectified colour airphotos, helped to delineate landslide geometry by examining vegetation distribution and scarp disturbance. A shaded-relief image of the LiDAR DEM with landslide boundaries generated in ArcMap is shown in Figure 3. Figure 4 shows the corresponding orthorectified airphoto image.

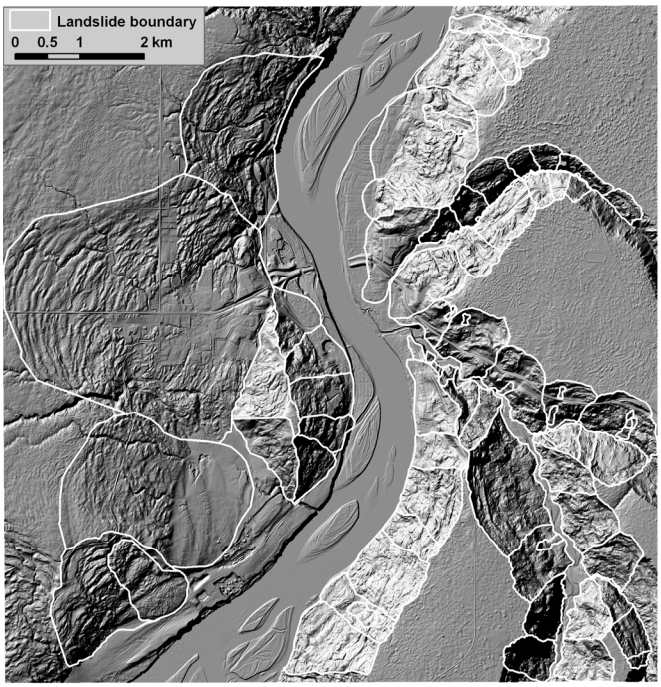

Figure 3. Landslide boundaries with LiDAR DEM. Study area UTM extent – top: 6236843, bottom: 6226338, left: 476028, right: 486198 (NAD83, zone 11).

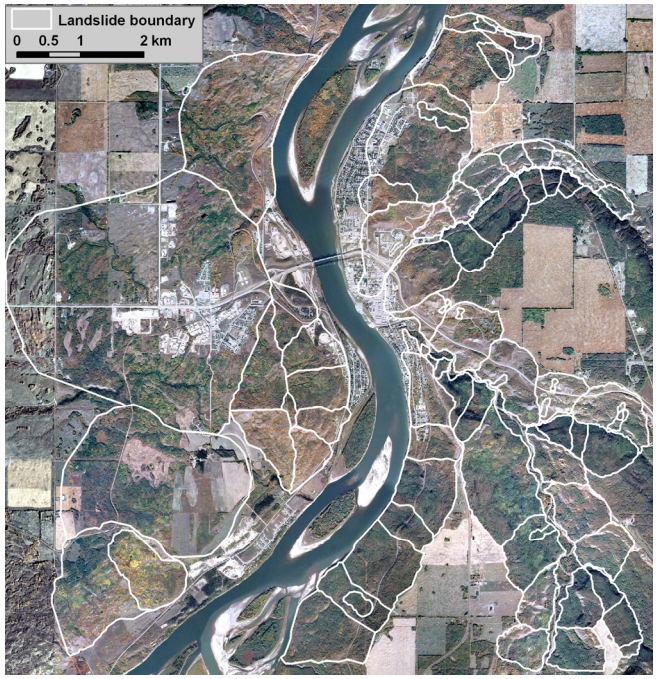

Figure 4. Landslide boundaries with airphoto imagery (created from 4 orthorectified airphoto images). Study area UTM extent – top: 6236843, bottom: 6226338, left: 476028, right: 486198 (NAD83, zone 11).

3.2 Landslide Classification

Classification of the landslide types in this report follows the suggested nomenclature developed by the UNESCO Working Party on World Landslide Inventory (1990; 1993; 1995) and Cruden and Varnes (1996). A brief explanation regarding the portions of the classification system used in this study follows.

Each landslide is assigned attributes based on the suggested type of movement (fall, topple, slide, spread, or flow) and the type of material (rock, debris, or earth). The landslides are also described based on activity, which has three components: state, distribution, and style. State has a number of options, including active, reactivated, suspended, and inactive. The inactive state is further subdivided to include dormant, abandoned, stabilized, and relict, depending on when the last movement event occurred. Distribution of the landslide is used to describe character as advancing, retrogressive, widening, enlarging, confined, diminishing, or moving, while the style descriptor has choices for complex, composite, multiple, successive, or single landslide events.

An additional descriptor, modifying condition, is also used in this landslide inventory. The two modifying condition options are anthropogenic activity, where man-made infrastructure is present on the slide mass, and toe erosion, for cases where a water course is eroding the toe of the slide. Table 1 lists the classification attributes assigned to each landslide polygon in the study area.

The slides on the valley slopes of the Peace River and tributaries are the result of river downcutting, so the majority of landslides in the study area have experienced multiple movements. It is difficult to determine how many movement events have occurred within one slide boundary. Because of this, classification only describes the movement type observed.

3.2.1 Morphological Classification

Morphological characteristics revealed in the LiDAR DEM, airphoto imagery, and field reconnaissance, as well as additional subsurface information gathered from an AGS borehole drilling program (Morgan et al., 2009), facilitate classification of the slides identified in the study area.

The LiDAR DEM was used to measure the dimensions of each landslide polygon. Landslide total length, width, and area were measured and recorded using ArcGIS. Slope angles were measured along the length of each landslide polygon. Overall slope angle is the average angle from the landslide main scarp or crown to the landslide toe. Slope angles were also measured for the depletion zone and accumulation zone of each slide.

A detailed examination of the stratigraphy at the project site (Morgan et al., 2012) identified a thick sequence of overconsolidated, rhythmically bedded sand, silts, and clays that were deposited as the Late Wisconsinan Laurentide Ice Sheet advanced into the region, blocking regional drainage and forming Glacial Lake Mathews within the ancestral Peace River valley (Hartman and Clague, 2008). Field reconnaissance at the study site indicated that the majority of deep-seated movement is occurring within this unit of horizontally bedded glaciolacustrine material, and examination of cross-sections derived from the LiDAR data corroborate the field observations (Morgan et al., 2012). For the purposes of this study, an average elevation of 435 m asl (derived from the cross-sections) was used as the dividing line between the accumulation zone and depletion zone.

Using these data sources, each landslide in the study area (shown in Figures 3 and 4) is classified according to type of movement, material involved, activity distribution, and style. The majority of landslides are classified as retrogressive, multiple, translational, earth slides. The full list of results are shown in Appendix 1, which contains the classification and measurements recorded for each discreet landslide polygon (Table 1) and also two key maps (Figures 14 and 15) relating the table information to each landslide.

Measured movement data derived from instrumentation installations at the study site are limited to a few specific and relatively shallow movement areas that affect infrastructure, and no monitoring data is

available for the deep-seated, large-scale movements discussed here. Because of this, a first pass estimation of the activity state of each defined landslide body was created based on visual evidence such as slope morphology, vegetative cover, and drainage observed using the airphoto imagery (Figure 3). It should be mentioned that although detailed monitoring information is limited, the historical record of movements at the townsite was also considered.

This visual approach to activity classification assumes that general vegetative cover and morphology is analogous to activity state. It is understood that vegetation type and cover are dependent on factors such as slope aspect and on the moisture profile of the slope. However, this preliminary visual classification considers disturbance to the vegetation as opposed to type of vegetation. This approach was used as a first pass for defining landslide activity prior to a more detailed examination using the LiDAR data.

Using the guidelines outlined in Section 3.2, and because landslides are well established in the area due to centuries of river downcutting, landslides with scarps bare of vegetation and with obvious signs of disturbance were given an activity classification of reactivated (Figure 5). Landslides that had well-developed drainage patterns and well-developed vegetation, vegetated scarps, or no obvious scarp disturbance were given an activity classification of relict (Figure 6). The relict descriptor refers to a landslide that clearly developed under different geomorphic or climatic conditions. Landslide surfaces that have well-developed vegetation or no obvious scarp disturbance, but the cause of the landslide remains apparent (e.g., undercutting of a riverbank by a watercourse), are given a classification of dormant, which assumes no movement within one year.

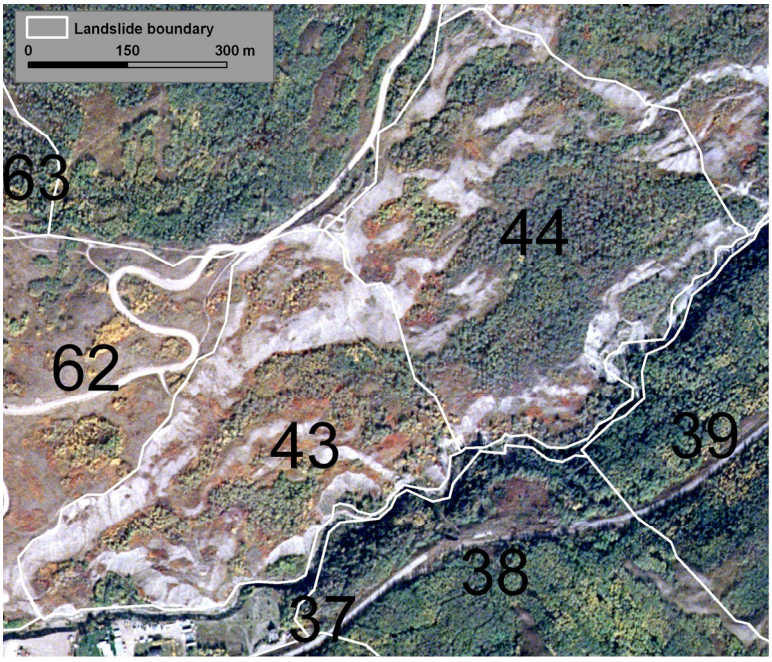

Figure 5. Two landslides, ID 43 and 44, assigned the activity classification 'reactivated' based on the vegetative and morphological characteristics observed in the airphoto. Note the large bare backscarps, which indicate landslide activity. Image is oriented with north pointing to the top of the page. UTM coordinates at centre of photo: 6233605N, 483045E (NAD 83, zone 11).

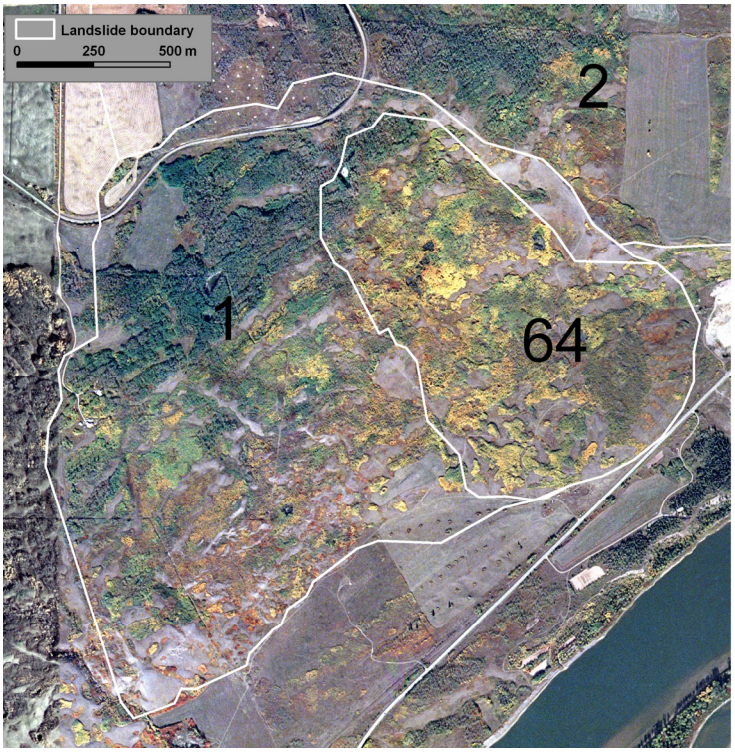

Figure 6. Two landslides, ID 1 and 64, assigned the activity classification 'relict' based on the vegetative and morphological characteristics observed in the airphoto. Note the Peace River (lower right of photo) no longer undercuts the toe of the landslide. Note also the well-developed drainage on the slope. Image is oriented with north pointing to the top of the page. UTM coordinates at centre of photo: 6227720N, 477880E (NAD 83, zone 11).

Figure 7. Two landslides, ID 15 and 16, assigned the activity classification 'dormant' based on the vegetative and morphological characteristics observed in the airphoto. Note the well-developed vegetation and absence of exposed or disturbed backscarp; the river is obviously the cause of the landslide. Image is oriented with north pointing to the top of the page. UTM coordinates at centre of photo: 6228990N, 482575E (NAD 83, zone 11).

3.3 Spatial Analysis

Topography is classified according to the methodology developed by Iwahashi and Pike (2006) and uses an unsupervised nested-means algorithm and a three part geometric signature to create slope angle, surface roughness, and local convexity derivative maps from the bare earth LiDAR DEM. We modified their methodology and applied additional analysis to our bare-earth LiDAR DEM to identify spatial relationships between these signatures. These analyses were performed using ArcGIS Spatial Analyst and Microsoft Excel.

3.3.1 Slope

Steepness of slope is an important landslide feature and is used in conjunction with field observations to help estimate the relative activity state of the slides in Peace River. We use the SLOPE function in ArcMap to develop derivative maps depicting ranges or classes of slope angle within the defined landslide polygons. Selection of these classes was based on a preliminary examination of landslide morphology made using airphoto imagery as discussed in Section 3.2.1.

To determine typical ranges of slope angle for each activity class, overall slope angle was measured along the length axis of each landslide polygon (the measurement axes are shown in Figure 15). Overall slope angle was then averaged for each activity state (relict, dormant, reactivated) assigned during the examination of the airphoto imagery. Average slope angle was also calculated for each activity state based on the modifying condition (anthropogenic activity or toe erosion). Results are shown in Figure 8. Based on these results average slope angles were assigned to each activity state to create non-overlapping ranges: less than or equal to 8°, greater than 8° to 12°, and greater than 12° representing the activity states relict, dormant, and reactivated, respectively.

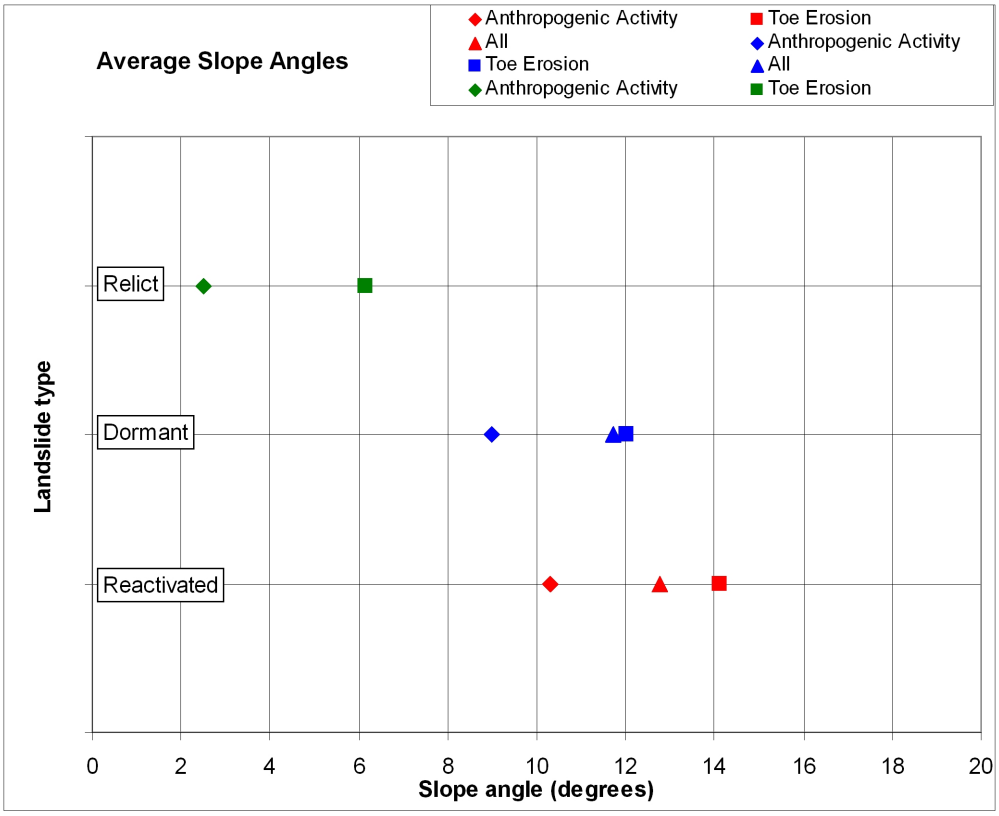

Figure 8. Range of average slope angles measured from the LiDAR DEM and sorted by visual airphoto classification.

The SLOPE function in ArcGIS analyses the bare earth LiDAR DEM using a 3×3 cell neighbourhood and compares the elevation of the middle cell to the elevation of surrounding cells to calculate slope angle. The slope analysis is applied to the area within the landslide polygons. Stable in situ areas such as vertical or near vertical outcrops are generally located outside the landslide polygons and are therefore not included in the analysis. Results are displayed with user-defined slope classes that encompass a range of slope angles. In comparison to the average angle analysis (Figure 8), which considers the average slope angle along a profile representing the length of a landslide, the SLOPE function creates a result that shows the distribution of slope angle, or slope gradient, across the landslide area and allows for a more complete understanding of slope angle distribution.

In this case, the typical ranges of slope angle determined from the average slope angle analysis (Figure 8) were used to define unique slope classes corresponding to the three activity states relict (≤ 8°), dormant (8 to 12°) and reactivated (>12°). Results are depicted on the slope gradient map shown in Figure 9. Many of the landslides that were classified as dormant using the airphoto analysis actually have a similar slope angle distribution to those landslides classified as reactivated using the same method. The slope gradient map was used to reclassify the activity state of each landslide using this more detailed picture of slope angle distribution. The refined classification identified two activity states across the project site, relict and re-activated, and the dormant classification was dropped.

Figure 9. Slope gradient classes used to reclassify activity state of landslides in the study area. Study area UTM extent – top: 6236843, bottom: 6226338, left: 476028, right: 486198 (NAD83, zone 11).

It became clear after examining the slope gradient map shown in Figure 9, that the slope analysis could be used to identify other slope classes to identify features of interest within each landslide. The analysis was run again using a fourth class that captured slopes greater than 20°. This class was defined based on field measurements of backscarp angle and was created to help identify their locations within each landslide. Figure 10 shows a slope gradient map with the red areas highlighting backscarp locations. A high concentration of these steep slopes within a landslide is a good indication of a reactivated activity state, although other data sources, if available, should also be considered before making the classification. It

should be noted that in some cases the steep slopes identified delineate the gullies created by drainage features.

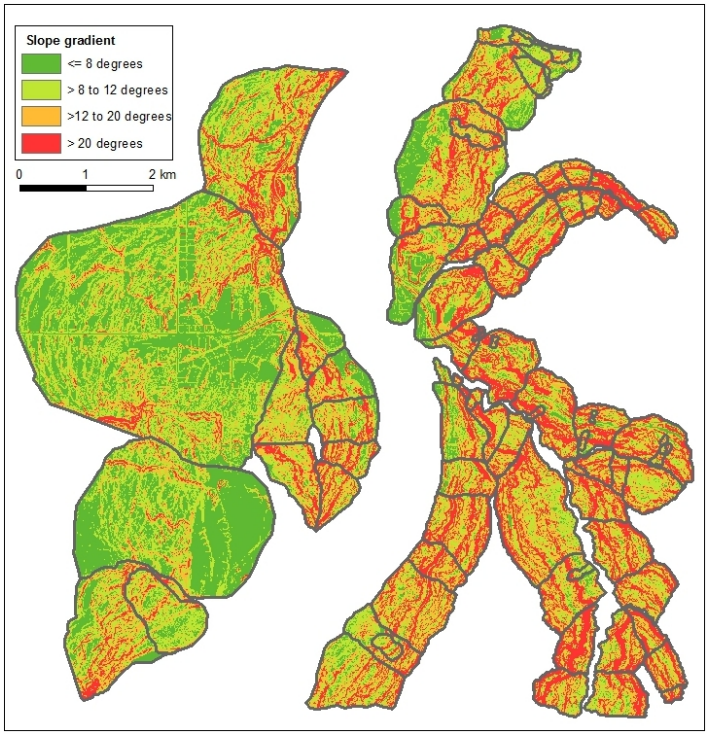

Figure 10. Slope gradient classes for landslides in the study area, with the addition of a fourth class (> 20°) used to identify backscarp locations. Study area UTM extent – top: 6236843, bottom: 6226338, left: 476028, right: 486198 (NAD83, zone 11).

This simple exercise highlights the usefulness of the slope analysis for comparing the morphological characteristics of landslides and also shows how airphoto analysis and slope analysis using the LiDAR DEM can sometimes produce differing interpretations. For best results, all data sources should be considered before making an activity state classification.

3.3.2 Surface Roughness

Surface roughness is used for identifying peaks and dips in a DEM by measuring changes in slope aspect and curvature of a cell from its surrounding cells (Iwahashi and Pike, 2007). It is achieved by comparing the elevation of each cell with its neighbouring cells. Generally speaking, a surface is considered to be rough when there is a high frequency of peaks and dips, and smooth when there is a low frequency. Surface roughness analysis ultimately compares the roughness of each landslide polygon to the roughness calculated for all landslide areas combined, effectively assessing a relative roughness.

The overall surface roughness is calculated by first creating a DEM derived from the LiDAR with a median filter (a 3×3 cell neighbourhood) to remove all the extreme high and low values or high-frequency spatial noise. Peaks were identified by subtracting this DEM from the LiDAR and were assigned a value of 0. Pits were identified by subtracting the LiDAR from the derived DEM and were assigned a value of 1. The sum of these two grids represents the distribution of peaks and pits.

The difference between this derived DEM and the original LiDAR DEM is used to generate a normalized surface that represents a roughness scale between 1 and 0, where 1 is smooth and 0 is rough. This scale describes the relative roughness at each 1 m cell location. A final roughness grid is then generated after passing the normalized surface through a mean filter with a 10 m radius to smooth out any residual noise.

The final grid resembles a shaded-relief DEM where smooth areas appear to be lighter than rougher areas, as defined by the selected colour ramp. To further differentiate the smooth areas from the rough areas, we grouped the roughness values into two classes (centred on the mean value of 0.4), with roughness values of 0.4 or lower representing rough surfaces and values higher than 0.4 representing smooth surfaces (Figure 11).

The steps for creating a roughness grid:

- Step 1: Create a derived (median) DEM from LiDAR with a 3×3 median filter.
- Step 2: Identify peaks if (LiDAR – derived DEM) > 0.
- Step 3: Identify pits if (derived DEM – LiDAR) > 0.
- Step 4: Combine peaks and pits to generate a new grid.
- Step 5: Use a 10 m radius mean filter to remove residual noise for determining surface roughness at each cell.
- Step 6: Use grid statistics to determine mean grid value of 0.4. Cells are classified as rougher than average if below or equal 0.4 and smoother when greater than 0.4.

The workflow for creating the roughness grid:

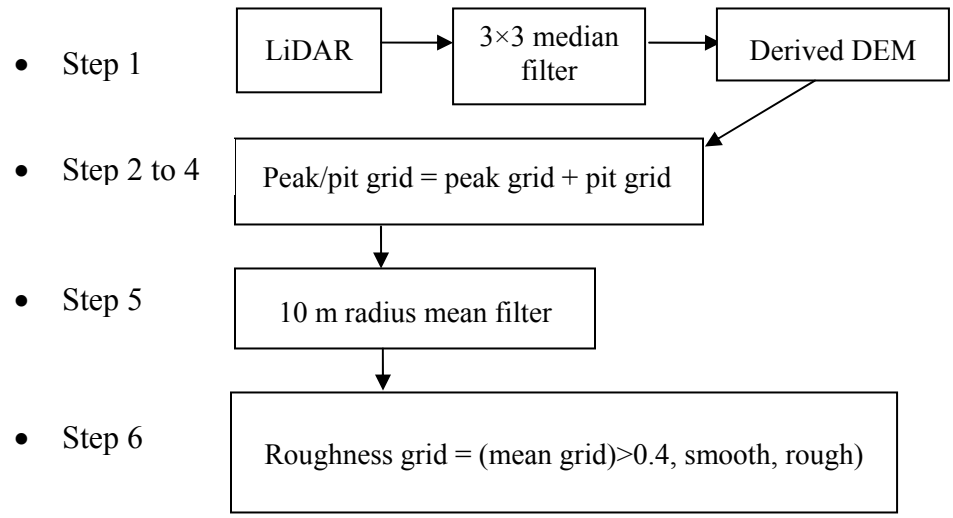

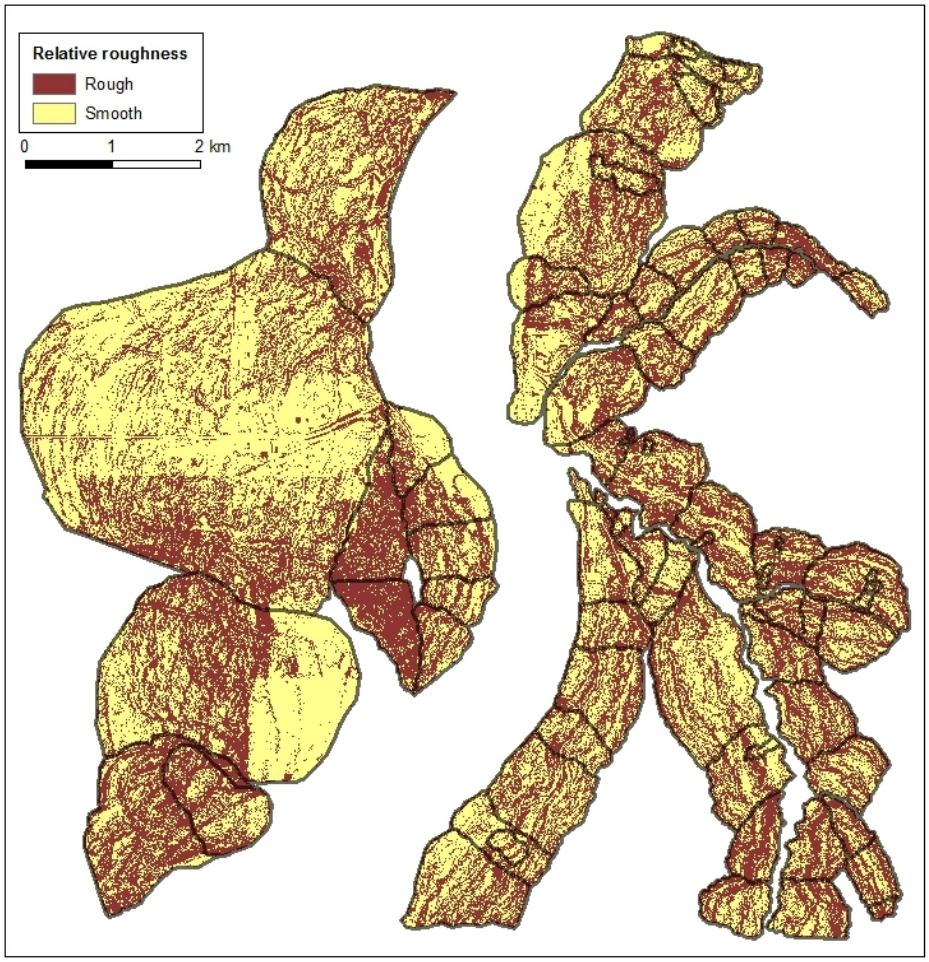

Figure 11. Relative roughness derivative map of the landslide areas. Study area UTM extent – top: 6236843, bottom: 6226338, left: 476028, right: 486198 (NAD83, zone 11).

3.3.3 Local Convexity

Local convexity measures the surface curvature, either convex or concave, of a landform. While slope gradient and surface roughness together are used to identify steep topography as potential landslide areas, convexity highlights differences among low-relief features, such as scarps of old and slow-moving landslide masses, from other landforms.

The CURVATURE function in ArcGIS is used to generate a curvature grid from the LiDAR DEM. The curvature grid is then normalized to values between 0 (concave) and 1 (convex). A mean filter with a 10 m radius is applied to smooth out any residual noise. The resulting convexity map shows that scarps from the old and slow-moving landslide masses are generally more concave than other active slides. After using a mean value of 0.5 to group all surfaces with values of 0.5 or lower as concave and higher than 0.5 as convex, a more distinct pattern of convexity starts to emerge (Figure 12).

The steps for creating a local convexity grid:

- Step 1: Use LiDAR as input to ArcGIS CURVATURE function.
- Step 2: Assign concave cells a value of 0 and convex cells a value of 1.
- Step 3: Use a 10 m radius mean filter to remove residual noise for determining local convexity.

- Step 4: Use grid statistics to determine mean grid value of 0.5. Cells are classified as concave if less than or equal to 0.5 and convex when greater than 0.5.

The workflow for creating a local convexity grid:

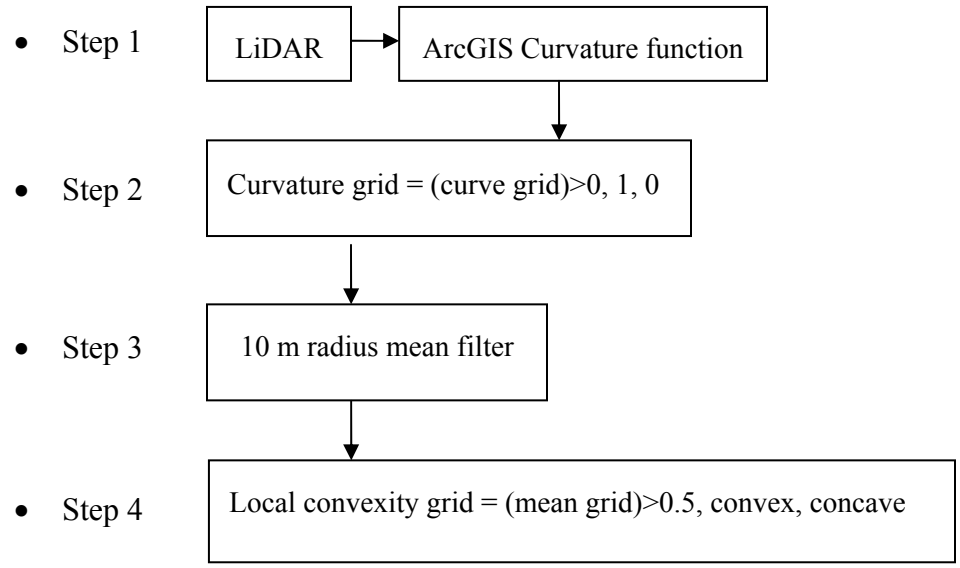

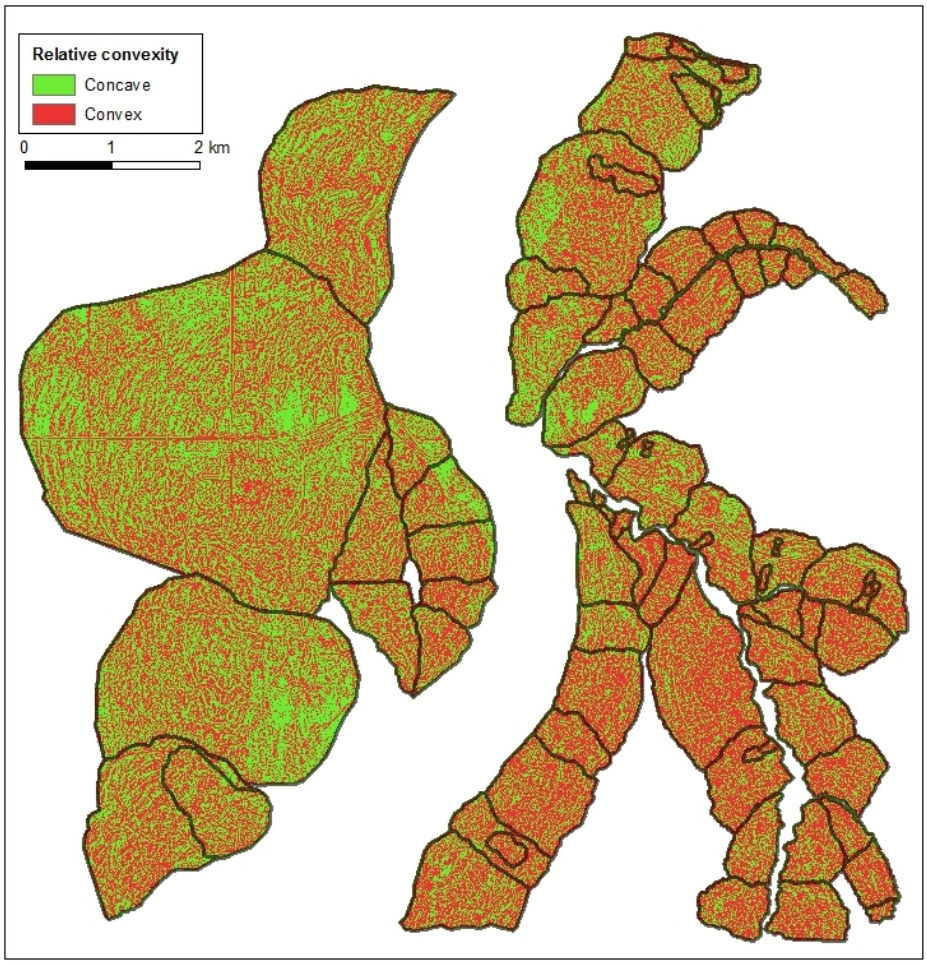

Figure 12. Relative convexity derivative map of the landslide areas. Study area UTM extent – top: 6236843, bottom: 6226338, left: 476028, right: 486198 (NAD83, zone 11).

3.3.4 Spatial Analysis Classification

As discussed in Section 3.2.1, airphoto imagery provides a means with which to make a preliminary assessment of landslide activity based on observations of vegetation types and cover and drainage patterns. However, this approach is somewhat limited as vegetative cover, especially stands of trees, can obscure the telltale morphological signs of movement that can so clearly be seen in a bare-earth LiDAR DEM. This is especially true for slow-moving landslides where small displacements over longer periods often do not greatly disturb the vegetative cover. The spatial analysis techniques of slope, relative roughness, and local convexity provide additional information to investigate the activity state of each slide relative to the others.

Classification of activity state in river valleys filled with glacial sediments is challenging due to the general state of instability created by thousands of years of river downcutting. Observing the subtle differences between the activity state of a landslide is further hampered by the lack of displacement data. In the absence of displacement data, we suggest that slope angle data can be used to assign a relative classification of activity state for each landslide across the study site. The slope calculation results depicted in the LiDAR-derived slope gradient map (Figures 9 and 10) provides a visualization of the distribution of slope angles. When reviewing this type of data, it is important to disregard the steep slopes created by drainage and concentrate instead on the distribution of main and minor backscarp slope angles.

In this study, scarps with slope angles greater than 12° were considered to indicate that the landslide is likely still moving, or reactivated. Relatively speaking, landslides that contain a greater number of backscarps, generally slopes greater than 20°, are considered to be experiencing the most displacement. Examination of the slope angle maps (Figures 9 and 10) indicate that landslides classified as dormant using the airphoto imagery method actually have a slope angle distribution meeting the reactivated criteria throughout the landslide body, and are therefore reclassified as reactivated for the purposes of the study. This reclassification also considers the landslide slope signature relative to slopes that are known to be moving.

The derivative maps depicting surface roughness and convexity were also reviewed to help determine the activity state of each landslide. Although they provided useful visual identification of relative surface texture of the defined landslides, they do not provide the compelling evidence that the slope gradient DEM does.

Application of this method resulted in two activity states in the study area, reactivated and relict. The distribution of activity states is shown in Figure 13. Table 1 also lists the activity state classification for each landslide using spatial analysis.

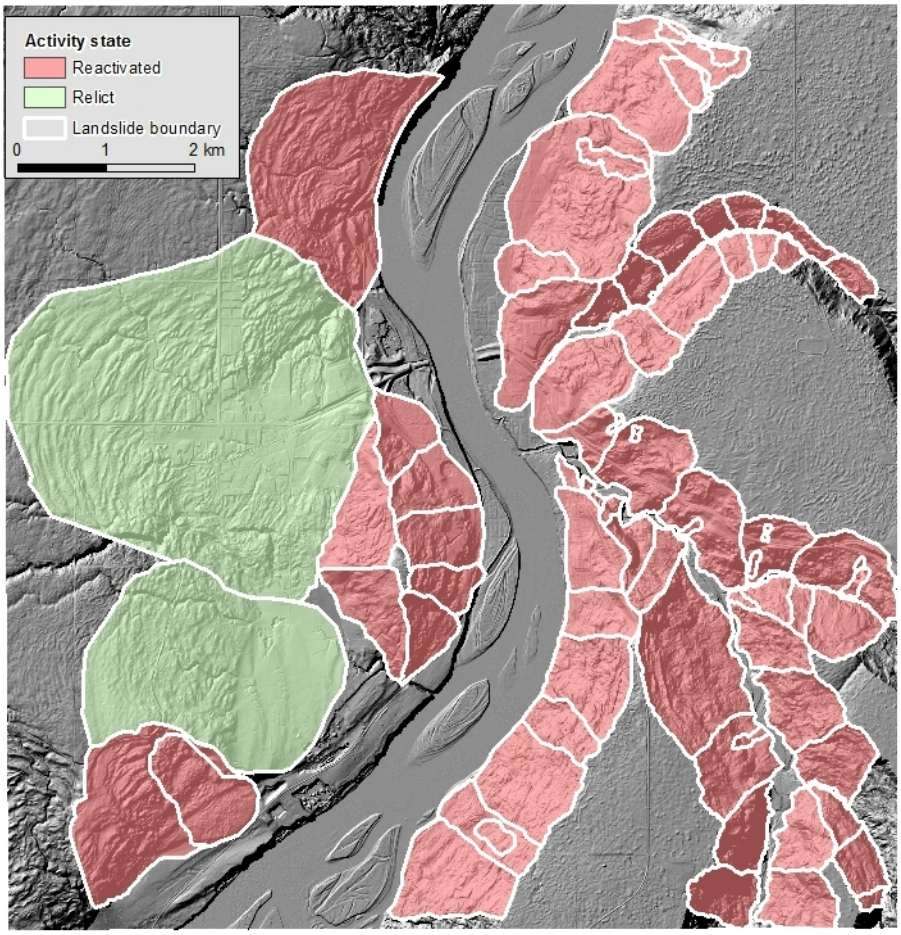

Figure 13. Activity state landslide distribution of the study area. Study area UTM extent – top: 6236843, bottom: 6226338, left: 476028, right: 486198 (NAD83, zone 11).

4 Discussion and Conclusion

This study provides a landslide inventory by classifying landslides in the Peace River study area based on morphological and spatial analysis of a high resolution LiDAR DEM. Classification follows the style suggested by Cruden and Varnes (1996). Data sources included airphoto imagery, LiDAR DEM, field reconnaissance, subsurface data, and GIS-based spatial analysis.

Due to the absence of displacement data for the large, deep-seated landslides being studied, spatial analysis techniques were used to select an activity state for each landslide. Three spatial methods were applied to the LiDAR DEM to derive maps depicting slope gradient, relative roughness, and relative convexity.

Slope gradient appears to be the most effective and informative method by which to classify the relative activity state of each landslide. Selection of activity state in this way is a somewhat subjective exercise without displacement data. However, the method does provide a reasonably repeatable method for choosing an activity state relative to the other landslides in the area. Until this method is refined further and perhaps combined more effectively with other spatial analysis methods, the selection of activity state is still somewhat subjective.

The selection of activity state using airphoto imagery resulted in a number of landslides being classified as dormant, based on vegetative cover and scarp disturbance. Reviewing these dormant classifications using the slope gradient derivative map derived from the LIDAR dataset reveals that these slides are more accurately described as reactivated based on the angles of the main and minor scarps and their similarity in slope angle and distribution to landslides where movement is known to occur. This process of landslide classification using multiple datasets highlights the limitations inherent in the selection of landslide activity using only one data source such as airphoto imagery, which relies on vegetative cover, as vegetative cover can be affected by other factors such as slope aspect and moisture content of the soil. This study has highlighted the benefit of having both imagery and a high resolution DEM for landslide classification.

Slope roughness and convexity maps are useful visual indicators of the surface texture of the defined landslides and, when used in conjunction with the other data sources, are useful when comparing landslides to assess relative levels of activity. However, on their own they have limited application for determination of activity state.

The spatial techniques used in this study provide a useful means to classify landslides in the absence of displacement data. However, in order to prove this method's usefulness, and to further investigate the usefulness of slope, roughness, and convexity in landslide classification, it is suggested that further research be conducted using a similar approach but in an area for which displacement data is available. If such a study proved that the spatial analysis approach is sound, the data could be used to calibrate or refine the approach.

5 References

Cruden, D.M. and Varnes, D.J. (1996): Landslides: Investigation and Mitigation; Transportation Research Board, National Academy of Science, Special Report 247, p. 36–75.

Hartman, G.M.D. and Clague, J.J. (2008): Quaternary stratigraphy and glacial history of the Peace River valley, northeast British Columbia; Canadian Journal of Earth Sciences, v. 45, no. 5, p. 549–564.

Iwahashi, J. and Pike, R.J. (2007): Automated classifications of topography from DEMs by an unsupervised nested-means algorithm and a three-part geometric signature; Geomorphology, vol. 86, p. 409–440.

Morgan, A.J., Slattery, S.R. and Froese, C.R. (2009): Results of sediment coring at the town of Peace River, northwestern Alberta (NTS 84C); Energy Resources Conservation Board, ERCB/AGS Open File Report 2009-18, 94 p.

Morgan, A.J., Paulen, R.C., Slattery, S.R. and Froese, C.R. (2012): Geological setting for large landslides at the town of Peace River, Alberta (NTS 84C); Energy Resources Conservation Board, ERCB/AGS Open File Report 2012-04, 41 p.

Pettapiece, W.W. (1986): Physiographic subdivisions of Alberta; Land Resource Research Centre, Research Branch, Agriculture Canada, scale 1:1 500 000.

UNESCO Working Party on World Landslide Inventory (1990): A suggested method for reporting a landslide; International Association for Engineering Geology, Bulletin 41, p. 5–12.

UNESCO Working Party on World Landslide Inventory (1993): A suggested method for describing the activity of a landslide; International Association for Engineering Geology, Bulletin 47, p. 53–57.

UNESCO Working Party on World Landslide Inventory (1995): A suggested method for describing the rate of movement of a landslide; International Association for Engineering Geology, Bulletin 52, p. 75–78.

Appendix: Landslide Inventory Details

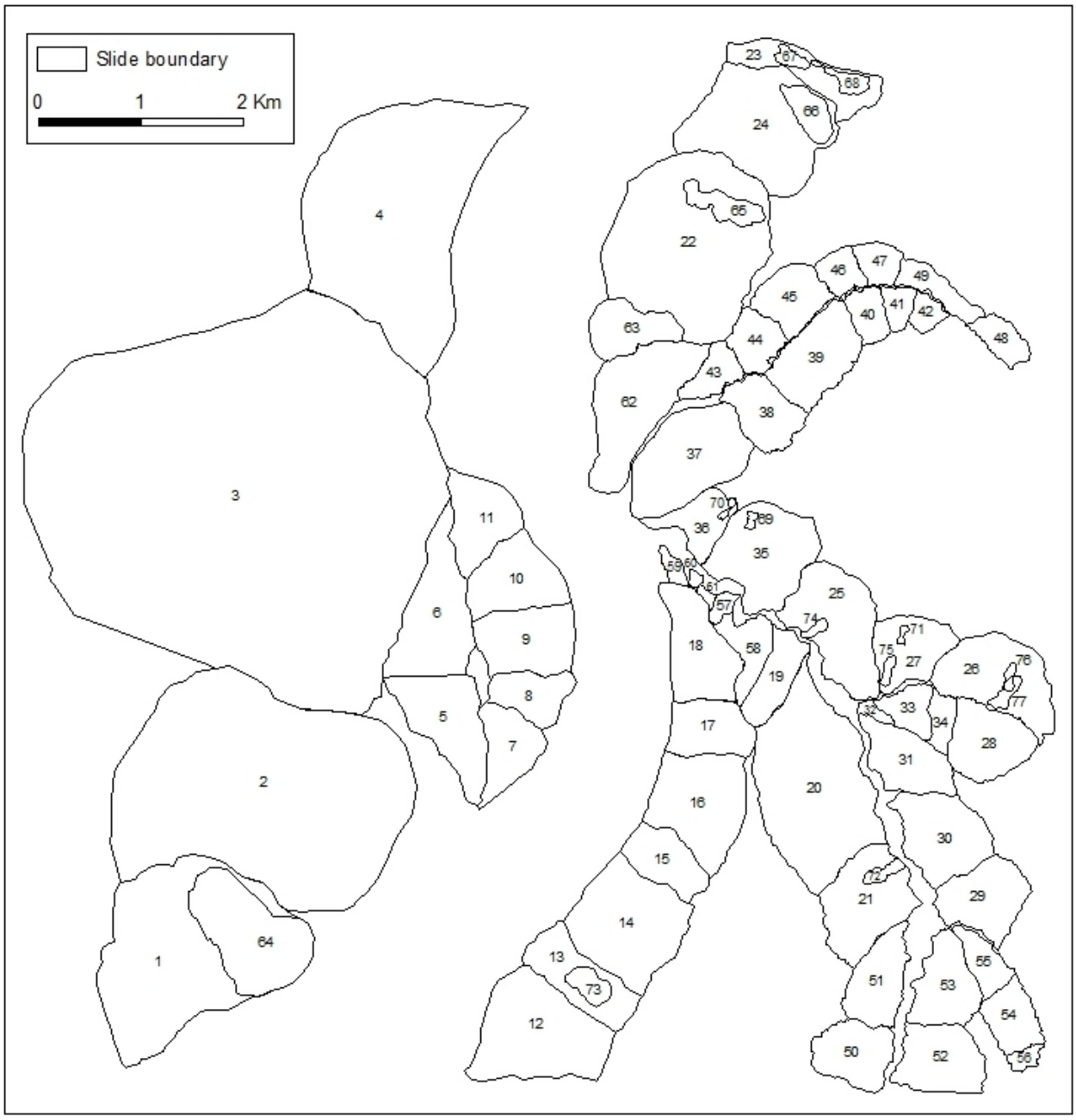

Figure 14. Landslide key map for use with Table 1. Study area UTM extent – top: 6236843, bottom: 6226338, left: 476028, right: 486198 (NAD83, zone 11)

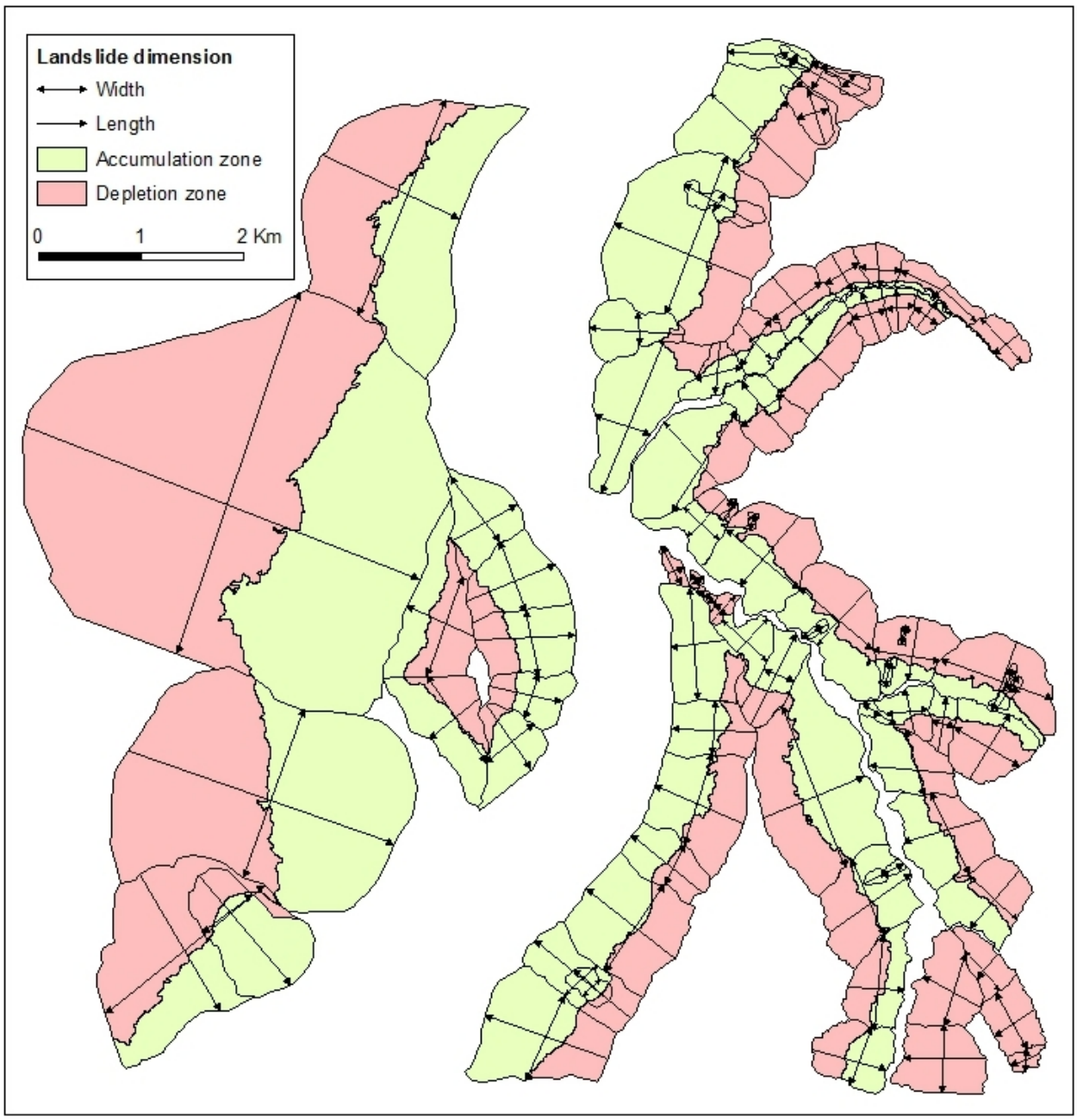

Figure 15. Measurement locations for landslide dimensions listed in Table 1 and the simplified accumulation/depletion zone boundary (435 m asl). Study area UTM extent – top: 6236843, bottom: 6226338, left: 476028, right: 486198 (NAD83, zone 11)

Table 1. Classification of landslide polygons at the study site as described in Section 3.2.

Id	Activity State	Modifying Condition	Distribution	Style	Material Type	Movement Type	Total Length[1] (m)	Width[2] (m)	Area (m^2)	Overall Slope Angle[3] (degrees)	Depletion Zone Angle[4] (degrees)	Accumulation Zone Angle[5] (degrees)
1	Reactivated	Toe erosion	Retrogressive	Multiple	Earth	Slide	1557	2000	2761147	6.2	8.5	9.3
2	Relict	Anthropogenic activity	Retrogressive	Multiple	Earth	Slide	2704	1814	5033788	3.2	7.3	4.8
3	Relict	Anthropogenic activity	Retrogressive	Multiple	Earth	Slide	4142	3717	12375756	1.8	4.5	2.4
4	Reactivated	Toe erosion	Retrogressive	Multiple	Earth	Slide	1495	2276	3395400	6.2	8.3	11.9
5	Reactivated	None	Retrogressive	Multiple	Earth	Slide	616	1059	682050	12.1	15.1	12.1
6	Reactivated	None	Retrogressive	Multiple	Earth	Slide	745	1063	830512	5.9	10.4	9.2
7	Reactivated	Anthropogenic activity	Retrogressive	Multiple	Earth	Slide	810	557	397177	11.6	19.4	12.0
8	Reactivated	Anthropogenic activity	Retrogressive	Multiple	Earth	Slide	738	452	324382	12.3	18.2	13.5
9	Reactivated	Anthropogenic activity	Retrogressive	Multiple	Earth	Slide	979	653	586511	9.4	11.9	10.6
10	Reactivated	Anthropogenic activity	Retrogressive	Multiple	Earth	Slide	943	719	559761	8.7	11.4	10.9
11	Reactivated	Anthropogenic activity	Retrogressive	Composite	Earth	Slide	733	538	491927	6.9	8.8	8.8
12	Reactivated	Toe erosion	Retrogressive	Multiple	Earth	Slide	1268	909	1079499	10.0	14.3	11.8
13	Reactivated	Toe erosion	Retrogressive	Multiple	Earth	Slide	1204	438	543797	10.0	16.0	9.0
14	Reactivated	Toe erosion	Retrogressive	Multiple	Earth	Slide	1111	1027	1016395	11.5	13.0	12.9
15	Reactivated	Toe erosion	Retrogressive	Multiple	Earth	Slide	886	440	373673	13.5	15.5	16.1
16	Reactivated	Toe erosion	Retrogressive	Multiple	Earth	Slide	939	925	827882	13.1	17.7	13.3
17	Reactivated	Anthropogenic activity	Retrogressive	Multiple	Earth	Slide	843	531	413400	12.8	18.0	13.0
18	Reactivated	Anthropogenic activity	Retrogressive	Multiple	Earth	Slide	545	1090	605631	11.4	14.0	14.0
19	Reactivated	Toe erosion	Retrogressive	Multiple	Earth	Slide	993	316	310839	10.0	14.2	12.1
20	Reactivated	Toe erosion	Retrogressive	Multiple	Earth	Slide	1065	1680	1754348	10.5	17.9	9.7
21	Reactivated	Toe erosion	Retrogressive	Multiple	Earth	Slide	990	808	722396	11.0	12.5	11.1
22	Reactivated	Anthropogenic activity	Retrogressive	Composite	Earth	Slide	1449	1647	2270170	8.4	14.2	8.9
23	Reactivated	Toe erosion	Retrogressive	Composite	Earth	Slide	1553	283	471051	7.7	10.3	8.6
24	Reactivated	Anthropogenic activity	Retrogressive	Composite	Earth	Slide	1289	1061	1314031	9.5	8.6	13.7
25	Reactivated	Toe erosion	Retrogressive	Composite	Earth	Slide	742	934	823880	14.3	15.5	20.8
26	Reactivated	Toe erosion	Retrogressive	Multiple	Earth	Slide	724	1153	752389	11.2	14.3	14.3
27	Reactivated	Toe erosion	Retrogressive	Composite	Earth	Slide	615	666	437719	14.3	14.3	23.1
28	Reactivated	Toe erosion	Retrogressive	Multiple	Earth	Slide	1553	280	500123	9.7	10.0	17.2
29	Reactivated	Toe erosion	Retrogressive	Multiple	Earth	Slide	744	650	512262	12.9	13.9	13.7
30	Reactivated	Toe erosion	Retrogressive	Multiple	Earth	Slide	801	877	629457	12.8	13.9	14.7
31	Reactivated	Toe erosion	Retrogressive	Multiple	Earth	Slide	849	661	452331	12.7	20.1	15.3

Id	Activity State	Modifying Condition	Distribution	Style	Material Type	Movement Type	Total Length[1] (m)	Width[2] (m)	Area (m^2)	Overall Slope Angle[3] (degrees)	Depletion Zone Angle[4] (degrees)	Accumulation Zone Angle[5] (degrees)
32	Reactivated	Toe erosion	Retrogressive	Multiple	Earth	Slide	387	98	41010	14.3	17.1	17.1
33	Reactivated	Toe erosion	Retrogressive	Multiple	Earth	Slide	445	410	193232	14.5	23.4	17.0
34	Reactivated	Toe erosion	Retrogressive	Multiple	Earth	Slide	539	230	127463	13.6	14.9	16.5
35	Reactivated	Anthropogenic activity	Retrogressive	Multiple	Earth	Slide	886	928	806361	12.5	13.9	15.3
36	Reactivated	Anthropogenic activity	Retrogressive	Multiple	Earth	Slide	548	468	299191	14.8	21.9	15.3
37	Reactivated	Anthropogenic activity	Retrogressive	Multiple	Earth	Slide	826	1167	898836	9.4	12.2	12.5
38	Reactivated	Toe erosion	Retrogressive	Composite	Earth	Slide	754	510	382777	11.6	15.8	17.4
39	Reactivated	Toe erosion	Retrogressive	Multiple	Earth	Slide	618	1004	575401	12.3	16.5	11.8
40	Reactivated	Toe erosion	Retrogressive	Composite	Earth	Slide	518	348	175779	13.0	13.5	16.5
41	Reactivated	Toe erosion	Retrogressive	Multiple	Earth	Slide	417	278	109705	15.2	15.0	23.3
42	Reactivated	Toe erosion	Retrogressive	Multiple	Earth	Slide	328	287	96840	17.9	18.3	18.2
43	Reactivated	Toe erosion	Retrogressive	Multiple	Earth	Slide	576	482	196324	13.8	21.3	18.1
44	Reactivated	Toe erosion	Retrogressive	Multiple	Earth	Slide	484	545	248234	14.5	22.7	16.7
45	Reactivated	Toe erosion	Retrogressive	Multiple	Earth	Slide	581	607	355149	12.5	13.0	19.1
46	Reactivated	Toe erosion	Retrogressive	Multiple	Earth	Slide	410	380	159398	16.1	15.7	27.5
47	Reactivated	Toe erosion	Retrogressive	Multiple	Earth	Slide	427	400	154332	15.4	14.1	28.9
48	Reactivated	Toe erosion	Retrogressive	Multiple	Earth	Slide	303	589	171047	18.4	18.2	18.2
49	Reactivated	Toe erosion	Retrogressive	Multiple	Earth	Slide	207	903	202190	27.9	27.4	26.7
50	Reactivated	Toe erosion	Retrogressive	Multiple	Earth	Slide	753	594	427240	13.5	20.2	11.4
51	Reactivated	Toe erosion	Retrogressive	Multiple	Earth	Slide	547	925	432292	18.9	27.8	23.0
52	Reactivated	Toe erosion	Retrogressive	Multiple	Earth	Slide	812	667	507933	12.7	15.9	15.9
53	Reactivated	Toe erosion	Retrogressive	Multiple	Earth	Slide	635	719	457078	16.0	17.3	17.3
54	Reactivated	Toe erosion	Retrogressive	Multiple	Earth	Slide	468	626	292135	16.2	17.1	17.1
55	Reactivated	Toe erosion	Retrogressive	Multiple	Earth	Slide	314	523	200892	20.0	21.9	21.9
56	Reactivated	Toe erosion	Retrogressive	Multiple	Earth	Slide	291	230	56380	20.8	22.3	22.3
57	Reactivated	Toe erosion	Retrogressive	Multiple	Earth	Slide	349	158	53423	15.4	*	*
58	Reactivated	Toe erosion	Retrogressive	Multiple	Earth	Slide	449	591	255295	13.5	*	*
59	Reactivated	Anthropogenic activity	Retrogressive	Multiple	Earth	Slide	165	422	56035	10.8	*	*
60	Reactivated	Toe erosion	Retrogressive	Multiple	Earth	Slide	149	161	17667	15.9	*	*
61	Reactivated	Toe erosion	Retrogressive	Multiple	Earth	Slide	93	199	21492	31.4	*	*
62	Reactivated	Anthropogenic activity	Retrogressive	Multiple	Earth	Slide	1614	570	932413	4.5	11.6	5.4
63	Reactivated	Anthropogenic activity	Retrogressive	Multiple	Earth	Slide	932	313	361504	8.1	13.9	10.7
64	Reactivated	Toe erosion	Retrogressive	Single	Earth	Flow	1398	610	909972	5.3	11.1	7.0

Id	Activity State	Modifying Condition	Distribution	Style	Material Type	Movement Type	Total Length[1] (m)	Width[2] (m)	Area (m^2)	Overall Slope Angle[3] (degrees)	Depletion Zone Angle[4] (degrees)	Accumulation Zone Angle[5] (degrees)
65	Reactivated	Toe erosion	Retrogressive	Single	Earth	Flow	772	201	166793	9.3	9.5	11.2
66	Reactivated	None	Retrogressive	Single	Earth	Flow	565	314	167182	7.1	9.6	9.6
67	Reactivated	None	Retrogressive	Single	Earth	Flow	321	132	46361	9.4	9.9	9.9
68	Reactivated	None	Retrogressive	Single	Earth	Flow	613	185	67194	7.2	7.6	7.6
69	Reactivated	Anthropogenic activity	Retrogressive	Single	Earth	Flow	163	97	13813	16.8	*	*
70	Reactivated	None	Retrogressive	Single	Earth	Flow	214	64	11582	18.5	*	*
71	Reactivated	Anthropogenic activity	Retrogressive	Single	Earth	Flow	188	87	12096	10.7	*	*
72	Reactivated	Toe erosion	Retrogressive	Single	Earth	Flow	425	104	47784	10.2	12.1	12.1
73	Reactivated	None	Retrogressive	Single	Earth	Slide	457	236	105590	10.8	13.7	10.3
74	Reactivated	Anthropogenic activity	Retrogressive	Composite	Earth	Flow	287	97	23957	17.6	*	*
75	Reactivated	None	Retrogressive	Multiple	Earth	Flow	302	95	26290	12.4	*	*
76	Reactivated	None	Retrogressive	Single	Earth	Slide	240	110	23264	9.5	*	*
77	Reactivated	Toe erosion	Retrogressive	Composite	Earth	Slide	387	148	49819	11.1	*	*

* These landslide polygons are located either above or below 435 m asl and therefore only overall slope angle has been recorded.

1 Total Length – minimum distance from toe of slide to crown

2 Width – distance between flanks of slide perpendicular to total length

3 Overall Slope Angle – calculated along the total length

4 Depletion Zone Angle – calculated along the total length from crown to 435 m asl elevation

5 Accumulation Zone Angle – calculated along the total length from 435 m asl elevation to the toe of slide